Title

Placental growth factor regulates the pentose phosphate pathway and antioxidant defense systems in human retinal endothelial cells.

Authors

Saddala, Madhu Sudhana
Lennikov, Anton
Huang, Hu

Publication Date

2020-04-15

DOI

10.1016/j.jprot.2020.103682

Peer reviewed

HHS Public Access

Author manuscript

J Proteomics. Author manuscript; available in PMC 2021 April 15.

Published in final edited form as:

J Proteomics. 2020 April 15; 217: 103682. doi:10.1016/j.jprot.2020.103682.

Placental Growth Factor Regulates the Pentose Phosphate Pathway and Antioxidant Defense Systems in Human Retinal Endothelial Cells

Madhu Sudhana Saddala[1], **Anton Lennikov**[1], **Hu Huang**[1,*]

[1]Mason Eye Institute, University of Missouri, Columbia, Missouri, United States of America

Abstract

The molecular mechanisms whereby placental growth factor (PlGF) mediates its effects in nonproliferative diabetic retinopathy (DR) are unknown. To better understand the role of PlGF in DR, we used tandem mass tags (TMT)-labeled quantitative proteomics to human retinal endothelial cells (HRECs), treated anti-PlGF antibody, and PBS as a control. Functional annotation and pathway enrichments were performed, which suggested that the differentially expressed proteins (DEPs) were involved in key metabolic processes, protein binding, and membrane, pentose phosphate pathway PPP and adherens junction. We conducted integrated gene profiles of our previously published transcriptomic data to the TMT-labeled proteomics data. The results showed the sixty proteins were found to be changed at the mRNA levels. The functional annotation conducted for the sixty proteins suggested that 58.3% of proteins were involved in PPP, 25% of proteins were in interleukin-12 singling and 16.7% of proteins were involved in glycolysis and gluconeogenesis pathway. Mass spec results were validated by transendothelial electrical resistance measurement by an electrical cell-impedance sensing and western blot analysis of VE-cadherin, G6PD. These findings suggest that the PPP proteins and antioxidants may act as a downstream target of PlGF and may play a decisive role in HREC biological functions in DR.

*Corresponding author: Hu Huang, PhD, University of Missouri, Dept. of Ophthalmology, School of Medicine, Mason Eye Institute, One Hospital Drive, Columbia, MO 65201, P: (573)882-9899, huangh1@missouri.edu.

Authors Contributions

The study was conceived and designed by MSS, AL, and HH. MSS performed data analysis, gene ontology, functional pathway analysis, and protein-protein network analysis. MSS and AL conducted mass spec samples, protein extraction, TEER, and western blot validation. The manuscript was written by MSS, AL, and HH, and critically revised by HH. All authors participated in drafting the manuscript, read and approved the final version of the manuscript.

Data availability

MS/MS data associated with the study were submitted to the PRIDE database (https://www.ebi.ac.uk/pride/archive/) and are available via ProteomeXchange with identifier PXD [*Deposition pending, the raw datasets identifier will be updated during the revision process*]

Competing interests

The authors have no competing interests.

Keywords

PlGF; Diabetic retinopathy; TMT-labeling; Proteomics; Pentose phosphate pathway; Retinal endothelial cells

Introduction

Placental growth factor (PlGF) was initially identified in human placental tissue and subsequently characterized as a member of the vascular endothelial growth factor (VEGF) family (1), (2). PlGF is known to play a pivotal role in pathological angiogenesis and inflammation by stimulating endothelial cell migration and by recruiting pericytes and inflammatory cells such as microglia and macrophages (3), (4), (5). PlGF demonstrates many features similar to those of VEGF and can directly interact with VEGF-A, producing PlGF/VEGF-A heterodimers. Clinically, PlGF is implicated in a variety of disorders associated with ischemia and angiogenesis. For example, reduced levels of PlGF caused by excessive release of soluble VEGFR1 (sVEGFR1) are a hallmark of preeclampsia (6). PlGF mediates therapeutic angiogenesis in myocardial infarction, diabetic wound healing, and limb ischemia (7). PlGF can also promote cancer angiogenesis and metastasis of cancer cells, suggesting that PlGF may be a potential target for cancer therapy (8). Additionally, PlGF may play a role in the pathogenesis of proliferative diabetic retinopathy (DR), as indicated by the observation that PlGF expression is increased in the vitreous of diabetic patients and that PlGF overexpression in the vitreous can cause characteristics of DR (9). Current evidence from animal experiments and clinical investigations suggests that PlGF can serve as a therapeutic target in the treatment of angiopathological disorders, particularly retinal vascular diseases such as neovascular, or “wet,” age-related macular degeneration (AMD), proliferative DR, and diabetic macular edema (DME) (10). Despite the well-defined pathophysiological roles of PlGF, the underlying molecular and cellular mechanisms are not completely understood, especially the exact relationships between biochemical events and molecular pathways regulated by PlGF, whose inhibition exhibits a protective role in DR.

Previously we reported that the absence of PlGF in diabetic $PlGF^{-/-}$ mice is associated with decreased expression of diabetes-activated hypoxia-inducible factor (HIF)1α (11) and inhibition of the VEGF signaling pathway, such as expression of VEGF, expression of VEGF receptor 1–3 (VEGFR1–3), and levels of phospho (p)-VEGFR1, p-VEGFR2, and p–endothelial nitric oxide synthase (5). Utilizing retinal proteome analysis, we also found that PlGF gene ablation inhibits the insulin resistance pathway and increases neuroprotective and antioxidant factors(12). Recently we have identified the roles of glucose-6-phosphate dehydrogenase (G6PD), peroxiredoxin-6 (Prdx6), and the pentose phosphate pathway (PPP) in the increased endothelial cell barrier functions that occur with PlGF inhibition via antibodies *in vitro*, including increased resistance, increased levels of junction and adherin proteins, and their reinforced cell membrane distribution (13).

In the present study, we used a quantitative tandem mass tags (TMT)-labelled proteomic approach, together with the comparison with the previously published transcriptomics (RNA Seq) data, to identify the differentially expressed genes (DEGs) and differentially expressed

proteins (DEPs) in HRECs treated with PlGF antibody and control HRECs treated with phosphate-buffered saline (PBS). Further bioinformatics analysis was performed to identify the enriched pathways among the DEGs and DEPs, which potentially act as downstream targets of PlGF signaling.

Materials and Methods

Cell culture and PlGF ab treatment

Primary HRECs were purchased from Cell Systems (Cat#: ACBR1 181, Kirkland, WA). HRECs were seeded on fibronectin-coated (10 μg/ml, overnight, 33016015, Gibco) plastic culture vessels and grown using the EBM-2 MV medium (Cat#: cc-4176, Lonza, Walkersville, MD) supplemented with 10% fetal bovine serum (FBS), 1% of penicillin/streptomycin (P/S), and EGM MV Singlequots growth supplement kit (Cat#: cc-4147, Lonza). Cells were used during passage 5 to 6. At about 80% confluence, the culture media was replaced with fresh media containing mouse anti-PlGF antibody (PL5D11D4; 25 μg/ml) and HRECs were collected 48 hours after the start of the incubation. PBS-treated cells were used as a negative control. We previously demonstrated the high affinity of the PL5D11D4 antibody with human PlGF using immune dot, and it's efficacy at 25 μg/ml concentration in HREC (13).

Protein extraction, digestion, and TMT-10 plex labeling

At the experimental endpoint, the control and PlGF-ab–treated HRECs were washed with PBS and lysed in a 2% of SDS in 50 mM Triethyl ammonium bicarbonate (TEABC) and phosphatase inhibitors 1 mM sodium fluoride (NaF), 2.5 mM sodium pyrophosphate, 1 mM sodium orthovanadate, and 1 mM β-glycerophosphate buffer, supplemented with a 1:100 protease inhibitor cocktail (Cell Signaling Technology); disruption of the tissue material was performed by a Q55 Sonicator (Qsonica, NY) with four pulses for 22 kHz, 5 s each at 30% power output on ice in the 4°C environment (cold room). Protein quantification was done by bicinchoninic acid (BCA) protein assay kit (Pierce, Waltham, MA), according to the manufacturer's instructions. Equal amounts of protein (1.5 mg) from control and PlGF-ab treated HRECs were taken, and sulfhydryl bonds in cysteine were reduced by dithiothreitol (DTT), 5 mM, and the mixture was incubated for 20 min at 60 °C. We performed a three-buffer exchange to reduce the concentration of the SDS from 2% to <0.05% by 8M urea buffer in 30 kDa MWCO filters (Millipore, Burlington, MA). Alkylation was carried out with iodoacetic acid (IAA), to a final concentration of 20 mM for 10 min at room temperature in the dark. The urea in the sample was further removed by buffer exchange with 50 mM TEABC buffer. Digestion of the proteins was performed with sequence-grade trypsin at a 1:20 ratio of trypsin to protein and incubated overnight at 37 °C. Peptides were vacuum dried until further use.

The resulting peptide mixtures were labeled with one of the TMT reagents from the 10plex version (Thermo Scientific, Rockford, IL), according to the manufacturer's protocol (14). TMT 10plex experiment was combined and acidified with trifluoroacetic acid to hydrolize the RapiGest surfactant. RapiGest was then removed according to the manufacturer's instructions, and the supernatants dried on a SpeedVac (15), (16). The labeled peptide

mixtures were desalted using C18 Macro Spin Columns (Harvard Apparatus). After peptide elution, samples were dried under vacuum. Peptides were then fractionated by off-gel electrophoresis (OGE) according to their pI on an Agilent 3100 OFFGEL fractionator (Agilent Technologies, Santa Clara, CA), following the manufacturer's manual. Isoelectric focusing was performed on a commercial 13 cm IPG pH 3–10 linear dry strip (GE Healthcare Biosciences AB, Uppsala, Sweden) with a 12-well frameset. After focusing, the 12 fractions were recovered individually and cleaned using C18 microspin columns (Harvard Apparatus, Holliston, MA). Eluted peptides were finally evaporated and stored at 20 °C prior to MS analysis.

LC-MS/MS analysis

The samples were then fractionated by high-pH reverse-phase high-performance liquid chromatography (HPLC) using an Agilent 300 Extend C18 column (5 μm particles, 4.6 mm ID, 250 mm length). The peptides were dissolved in 0.1% formic acid (FA) and directly loaded onto a reversed-phase precolumn (Acclaim PepMap 100, Thermo Scientific, Rockford, IL). Peptide separation was performed using a reversed-phase analytical column (Acclaim PepMap RSLC, Thermo Scientific). The gradient was comprised of increasing solvent B (0.1% FA in 98% ACN), from 8% to 26% in 22 min, 26% to 40% in 12 min, and 40% to 80% in 3 min, and then holding at 80% for the last 3 min, all at a constant flow rate of 400 μl/min on an EASY-nLC 1000 UPLC system. The resulting peptides were analyzed by a Thermo Scientific™ Q Exactive™ plus hybrid quadrupole-Orbitrap mass spectrometer (Thermo Fisher Scientific, Waltham, MA). The peptides were subjected to nanospray ionization (NSI) source followed by tandem mass spectrometry (MS/MS) in Q Exactive™ plus (Thermo Fisher Scientific, Waltham, MA) coupled with the ultra-high-performance liquid chromatography (UPLC) (17). Intact peptides were detected in the Orbitrap at a resolution of 70,000. Peptides were selected for MS/MS using the nanospray collision energy (NCE) setting as 30; ion fragments were detected in the Orbitrap at a resolution of 17,500 (18). A data-dependent procedure that alternated between one MS scan followed by 20 MS/MS scans was applied for the top 20 precursor ions above a threshold ion count of 1E4 in the MS survey scan with a 30.0 s dynamic exclusion. The electrospray voltage applied was 2.0 kV. Automatic gain control (AGC) was used to prevent overfilling of the Orbitrap; 5E4 ions were accumulated for the generation of MS/MS spectra. For MS scans, the m/z scan range was 350–1800. The fixed first mass was set as 100 m/z.

Proteomics data analysis

Data analysis was performed on Proteome Discoverer 2.4 (Thermo Fisher Scientific) using Sequest and Mascot search engines and the MaxQuant tool program (http://www.maxquant.org) (12). The data were searched against the National Center for Biotechnology Information (NCBI) human reference sequence (NCBI RefSeq) protein database containing 71,644 protein sequences (https://www.ncbi.nlm.nih.gov/refseq/) (19). The fixed modification included in the search parameters were the carbamidomethylation of cysteine, TMT 10-plex labels at the N-terminal of the peptide (229.16 Da), and a lysine side chain (229.16 Da). N-terminal acetylation, oxidation of methionine, phosphorylation at serine, threonine, and tyrosine (+79.966 Da), and were included in the algorithm as variable modification. MS/MS was searched with a precursor mass tolerance of 10 ppm, and the

fragment mass tolerance was set to 0.05 Da. The protease used was specified as trypsin, and a maximum of two missed cleavages was allowed. The data were searched against a target decoy database, and the false discovery rate was set to 1% at the peptide level. The TMT ratio for each peptide–spectrum match was calculated by the quantitation node, and the probability of phosphorylation for each Ser/Thr/Tyr site was calculated by the phosphoRS3.1 node in the Proteome Discoverer and MaxQuant programs. Only the phosphopeptides with >75% site localization were considered for the analysis. The peptides with ratios of ≥1.5 in at least three samples were considered as significant differentials and used for further data analysis.

Gene Ontology Analysis

The GO annotation proteome was derived from the UniProt-GOA database (http://www.ebi.ac.uk/GOA/). GO annotation contains three categories: biological process, cellular compartment, and molecular function. For each category, a two-tailed Fisher's exact test was employed to test the enrichment of the differentially expressed protein against all identified proteins. Correction for multiple hypothesis testing was carried out using standard FDR control methods. GO terms with a corrected p-value < 0.05 were considered significant. The KEGG database was used to annotate the protein pathways. First, we used the KEGG online service tool KAAS (Kregg Automatic Annotation Server) to annotate the protein's KEGG database description. Then, we mapped the annotation result on the KEGG pathway database using the KEGG online service tool KEGG mapper.

Protein-protein network analysis

Protein-protein network analysis was performed for 60 overlap DEPs by using the STRING (Search Tool for the Retrieval of Interacting Genes) database (https://string-db.org/) to disclose possible connections among proteins and to visualize the PPI (protein-protein interaction) network. The PPI network was constructed by setting the minimum required interaction score to medium confidence (0.4). The active interaction sources included were experiments and text mining. The setting parameters for a maximum number of interactors to show for first shell and second shell were, respectively, none/query protein only and none. GO functional enrichment analyses of proteins in the PPI network were directly performed online to retrieve GO terms assigned to a set of proteins in the GO categories of molecular function, biological process and cell component with an FDR < 0.05 on the whole genome background (20). The overall study design is depicted in Figure 1.

Transendothelial electrical resistance measurement by an electrical cell-impedance sensing

Experiment was performed as described previously (13). Briefly, the primary HRECs were seeded on an 8-well electrical cell-impedance sensing (ECIS) array and cultured as described above. Transendothelial electrical resistance (TEER) was monitored with the ECIS system (Applied BioPhysics, Troy, NY, USA) in real-time every 10 minutes at 4 kHz AC frequency.

Western blot validation

Western blot (WB) validation of cellular protein extracts was performed, as was previously described (13). The protein concentration was determined with the Qubit 4 Fluorometer (Thermo Fisher Scientific). Thirty micrograms of total protein were separated on the SDS-PAGE gel and further transferred to membrane for immunoblotting assay. Membranes were blocked with 5% nonfat milk (Bio-Rad) at room temperature for 1 h and then incubated overnight at 4°C with the primary antibodies: anti-vascular endothelial (VE)-cadherin (1:1000, 5012896; Thermo Fisher Scientific), anti-G6PD (1:500, MA5–15918; Thermo Fisher Scientific), β-actin (PA1–21167; 1:2,000; Thermo Fisher Scientific). The target protein bands were detected with HRP-conjugated IgG antibody (172-1011, 1:1,000; Bio-Rad), which was visualized by chemiluminescence with Clarity Western ECL substrate (Bio-Rad) and imaged using the LAS-500 Imaging System (General Electric, CT, USA). The resulting band sizes were resolved using Precision Plus Protein™ Kaleidoscope (Bio-Rad) protein standard.

Statistical analysis

Student's t-tests and Benjamini–Hochberg corrections (FDR) were used. A *p*-value of less than 0.05 was considered significant. The biological replicates were performed for control and PlGF-ab– treated and proteomic differences were evaluated for statistical significance ($P < 0.05$) by Student's t-tests, and corrected for multiple testing using the Benjamini–Hochberg correction. Means were calculated for the biological replicates, and fold changes were determined by dividing the mean intensity value of the control samples by that of the PlGF ab treated samples for each protein. The fold change was transformed using the log2 function so that the data is centered around zero, while the Benjamini–Hochberg corrected *p*-value was-log10 transformed for volcano plot scaling.

Results

Identification of differentially expressed proteins (DEPs)

We used a TMT-based quantitative proteomic method to identify the proteome changes in HRECs treated with PBS (control) and PlGF-ab. The overall study design is depicted in Figure 1. The upstream TMT labeling of mass spectrometric analysis allows for multiplexed relative protein quantification of multiple samples in one single liquid chromatography-mass spectrometry tandem MS (LC-MS/MS) analysis so that the technical variations between different experiments could be overcome (21). The five control and five PlGF-ab–treated HREC protein extracts were processed for quantitative proteomics analysis using TMT labeling. LC-MS/MS, followed by bioinformatics analysis, identified a total of 7,286 proteins from control and PlGF-ab–treated groups, which was quantified by multiple peptides at an initial protein false discovery rate (FDR) of less than 1%. Initial analysis identified 685 proteins that demonstrated significantly different quantities between the control and PlGF-ab-treated samples.

We applied the Benjamini–Hochberg method (22) to correct for multiple testing, which reduced the number of differentially abundant proteins to 305. The 305 proteins were considered the final DEPs between the control and PlGF-ab–treated groups, with p-value

<0.05 and the maximum absolute value of fold change ≥0.2 (based on ANOVA analysis). Hierarchical clustering analysis of the 305 DEPs illustrated the overall consistency of up- and down-regulation between the two groups. The DEPs were designated to be significantly regulated, as demonstrated by the Student's t-test (p-value ≤ 0.05) and relative fold change (FC) from DEPs of control HRECs as compared to DEPs of HRECs subjected to PlGF-ab treatment (FC ≤ 0.23). Principle component analysis (PCA) and volcano plot were performed to graphically represent the quantitative data as a sample distribution (Supplementary material, Figure 1).

Gene ontology and functional classification of the DEPs

The DEPs were uploaded to the DAVID (Database for Annotation, Visualization, and Integrated Discovery) annotation tool (https://david.ncifcrf.gov/) and Panther classification system database (23), (20), with the complete human genome as the background for gene ontology (GO) classification. We have investigated the biological process, cellular component, molecular function, protein classes, and functional pathways in the significantly enriched GO terms.

The significant upregulation of proteins in the PlGF-ab–treated group, was primarily related to protein production and regulation. The biological process classification revealed that the DEPs are involved in the metabolic process (22.63% of DEPs), regulation of biological process (20.75%), response to a stimulus (13.67%), cell organization and biogenesis (13.11%), transport (10.07%), and other activities (19.77%). Most of the DEPs are involved in the metabolic process (22.63%) and regulation of biological process (20.75%) (Figure 2A). The molecular function results revealed that the DEPs are involved in protein binding (33.95%), RNA binding (8.50%), DNA binding (5.42%), catalytic activity (19.07%), nucleotide-binding (7.71%), metal ion binding (9.70%), and other activities (15.64%). Most of the DEPs are involved in protein binding (33.95%) and catalytic activity (19.07%) of molecular functions (Figure 2B). The cellular component results revealed that the DEPs are involved in the membrane (18.80%), nucleus (15.80%), mitochondrion (5.35%), cytosol (15.98%), cytoplasm (15.54%), and other activities (28.52%). Most of the DEPs are involved in the membrane (18.80%) and other (28.52%) of cellular components (Figure 2C). The protein classification results revealed that the DEPs go to various classes like transferase (22.1%), cytoskeletal protein (13.5%), enzyme modulator (17.3%), hydrolase (18.3%) and nucleic acid binding (28.8%). Most of the DEPs belong to nucleic acid binding (28.8%) and transferase (22.1%) of protein classes (Figure 3A).

The DEPs were further subjected to pathway-focused functional analysis. The results showed that most of the identified proteins are involved in the PPP (10 proteins), adherens junction (6 proteins), p53 signaling pathway (5 proteins), signal transduction of sphingosine-1-phosphate (S1P) receptor (4 genes), Alzheimer disease–presenilin pathway (6 genes), metabotropic glutamate receptor group III pathway (4 genes), antifolate resistance (4 genes), and one-carbon metabolism (4 genes) (Figure 3B). The functional pathway results revealed that most of the DEPs are involved in the PPP (23%), adherens junction (14%), and Alzheimer's disease–presenilin pathway (14%).

Comparative analysis of Proteome and Transcriptome

Despite the central dogma of gene expression from mRNA transcription to protein translation, protein changes often cannot be matched with their mRNA transcript changes due to post-transcriptional modifications and spatiotemporal dynamics of mRNA transcripts. Therefore, we performed a comparative analysis of the current proteome and previously published transcriptomic (RNA Seq) data (24), which identified a total of 53,808 significant transcripts from the raw datasets of 12 files (6 controls vs. 6 treatments). Among them, a total of 3,275 DEGs that satisfy q-value (FDR-corrected p-value) < 0.05 and fold change ≥ ±2.0, were identified in the PlGF-ab–treated HREC samples relative to the control HREC samples. These DEGs were compared with DEPs from proteomics analysis by the Venny tool (https://bioinfogp.cnb.csic.es/tools/venny/) (12). Sixty DEPs were found to their matched mRNA transcripts in the DEGs (Figure 4). Functional analysis and classification were further performed for these 60 overlap transcripts/proteins (Figure 5). The results showed that they are involved in the PPP (58.3%), interleukin-12 signaling (25%), and glycolysis, and gluconeogenesis (16.7%). Both datasets indicated that the majority of proteins/transcripts were involved in PPP, such as aldolase A (ALDOA), aldolase, fructose-biphosphate C (ALDOC), deoxyribose-phosphate aldolase (DERA), glucose-6-phosphate dehydrogenase (G6PD), 6-phosphogluconolactonase (PGLS), transketolase (TKT), and retinal pigment epithelium (RPE) (Table 1). The results suggest that the PPP may play an essential role in the protective effect provided by PlGF in HRECs.

Protein-protein network analysis of the pentose phosphate pathway proteins

We further analyzed the seven PPP elements that overlap between the DEGs and the DEPs. All of the seven proteins were used for the protein-protein interaction analysis with the human genome as the background using the STRING database (https://string-db.org/). We constructed five various networks, including evidence-based network, confidence-based network, molecular action-based network, molecular action-based k means clustering, molecular action based Markov Cluster (MCL) clustering (Figure 6). All the networks have 7 nodes, 18 edges, 5.14 average node degree, 0.886 average local clustering coefficient, and 0 expected number of edges with a PPI enrichment p-value < 1.0e-16. The evidenced-based network showed that all the genes were directly connected, and ALDOC (red color sphere) was the query protein and first interactor. Interestingly, the G6PD gene was shown to interact with many genes, such as ALDOA, ALDOC, DERA, PGLS, TKT, and RPE (Figure 6A). Based on confidence analysis, G6PD showed the highest interaction with ALDOA, ALDOC, DERA, PGLS, TKT, and RPE (Figure 6B). The molecular action network was also performed to gain insights into how these genes affect each other, and the results reveal that G6PD binds directly with ALDOA, ALDOC, DERA, PGLS, TKT, and RPE (Figure 6C). The molecular action-based k-means clustering network results showed that the clustering of the seven proteins involved in the PPP exhibited three distinctive clusters. In one cluster, proteins, G6PD, and PGLS were grouped (green color), while ALDOA and ALDOC clustered together (blue color), and DERA, TKT, and RPE clustered with each other (red color) (Figure 6D). The molecular action-based MCL clustering network analysis showed the clustering of the seven proteins involved in the PPP. The seven proteins were clustered together (Figure 6E). All the networks of Kyoto Encyclopedia of Genes and Genomes

(KEGG) pathway showed that 7 of 30 genes and Reactome pathways identified, 5 of 15 genes to be involved in the PPP.

Treatment with anti-PlGF antibody increased the barrier function of HREC and G6PD expression in HREC lysates.

Both TEER data (Figure 7A) and western blot analysis (Figure 7B) indicated that inhibition of PlGF resulted in increased resistance of HREC monolayer and elevated expression of VE-Cadherin suggestive of increased endothelial barrier function when treated with ani-PlGF antibody, these results are consistent with our mass-spec and RNA-seq findings as well as previous experiments (25). Consistent with our findings in mass-spec and RNA-seq results. G6PD upregulation by the anti-PlGF antibody at 48 h was also validated by western blot analysis (Figure 7B). Previously we reported increased expression of Prdx6 in PlGF-ab treated HREC (13).

Discussion

The present study employed a TMT-based proteomics approach to identify the total protein in HREC protein lysates and quantify the protein expression differences in the presence and absence of PlGF signaling. A total of 7,286 proteins were identified in HREC protein extracts, and 305 proteins were found to differentially express between the control and PlGF-ab treatment samples. DEPs were further characterized and annotated for gene ontology and functional enrichment analyses. The complete set of proteins and pathways regulated by PlGF signaling in HRECs were identified at the genomic level. Identification of such DEPs/DEGs gives novel insights into the mechanisms whereby PlGF is involved in vascular endothelial cell functions, such as proliferation, angiogenesis, and barrier function, and provides new candidates for function evaluation and new targets for potential therapeutic intervention of vascular disorders, such DR and DME.

Pathway-focused bioinformatics analysis demonstrated that the PPP, such as ALDOA, ALDOC, DERA, G6PD, PGLS, phosphoglucomutase-1 (PGM1), phosphoglucomutase-2 (PGM2), RPE, transaldolase-1 (TALDO1), and transketolase (TKT), is one of the involved pathways in HRECs and may play a beneficial role in diabetes-related oxidative damage to retinal cells since it is the primary source of reductant co-factor nicotine adenosine dinucleotide phosphate (NADPH). Oxidative stress is caused by an imbalance between the antioxidant defense system and the production of reactive oxygen species (ROS). The PPP catalyzes the oxidative decarboxylation of glucose-6-phosphate (G6P), conserving its redox potential relying on nicotinamide adenine dinucleotide phosphate ($NADP^+$); thus, by two sequential reactions, which are catalyzed by G6PD and 6-phosphogluconate dehydrogenase (6PGD), respectively, 2 mol of NADPH is generated from 2 mol of $NADP^+$ per mol of the oxidized G6P. The oxidative branch of PPP yields ribulose-5-phosphate (R5P), which isomerizes to ribose-5-phosphate and can be used for nucleotide biosynthesis (26). Depending on the cellular context, some R5P molecules can be recycled to the glycolytic intermediates fructose-6-phosphate (F6P), which can be isomerized back to G6P, and glyceraldehydes-3-phosphate (G3P) by the non-oxidative PPP branch. The G6PD gene plays a crucial role in regulating carbon flow through the PPP. Specifically, the enzyme affects the

production of the reduced form of the extramitochondrial NADPH coenzyme by controlling the conversion of G6P to 6-PGD in the PPP. Our results in the PlGF-ab–treated HRECs suggest that the G6PD protein is up-regulated in the absence of PlGF and stimulates the oxidative branch of PPP to supply cytosolic NADPH to counteract oxidative damage as well as up-regulating antioxidant proteins such as Prdx6, NQO1, and YES1. Our previous proteomics studies also reported that PlGF knockout increases antioxidant proteins (e.g., Prdx6) and neuroprotective proteins (e.g., Map2) in the diabetic mouse retina (12).

The comparative analysis of proteome and transcriptome revealed the alteration of the expression of 60 genes at both mRNA and protein levels. The functional analysis revealed that 58.3% of these common gene products are involved in the PPP, such as ALDOA, ALDOC, DERA, G6PD, PGLS, RPE, and TKT. In order to verify their interactions, regulatory networks were constructed. Interestingly, the seven PPP gene products were the most critical hubs orchestrating protein regulation in the constructed molecular action-based (MCL clustering) regulatory network. ALDOA, aldolase fructose-bisphosphate B (ALDOB), and ALDOC are three members of the aldolase isozyme family, are encoded by separate genes (27) and are involved in one of the essential steps in glycolysis, a process required in all cells that consume glucose (28). The three proteins are expressed in a tissue-restricted manner (29). For example, ALDOA is the key enzyme of the glycolytic pathway and is virtually ubiquitous in all mammalian tissues, including the brain, and in all cell types of the retina (30). The transcriptomic analysis also revealed that the PPP is up-regulated by PlGF-ab in HRECs. Further pharmacological inhibition and gene silencing by siRNA confirmed that PlGF inhibition promotes endothelial cell barrier function and prevents endothelial cell dysfunction by high glucose through activation of G6PD and PPP, as well as antioxidant defense (13)

The PPP plays a beneficial role in protecting the cells against oxidative stress by the production of NADPH. Antioxidant systems such as peroxiredoxins (PRDX) family members (e.g., PRDX1, PRDX3, and PRDX6) and the Nrf2-antioxidant responsive element (ARE) pathway (e.g., heme oxygenase 1 [HMOX1], NQO1, and YES1) were regulated by PPP and can prevent endothelial cell barrier dysfunction by oxidative stress in diabetes (13). Our current and previous findings indicate that the PlGF inhibition promotes HREC biological functions through the antioxidant defense and the PPP, which acts as a downstream target pathway and is implicated in the pathophysiology of DR.

Conclusion

In conclusion, A total of 305 proteins were found to be differentially expressed between the PBS-treated HREC control samples and PlGF-ab–treated HREC samples. Among them, the expression of 60 genes was altered at both mRNA and protein levels. These DEPs are involved in the PPP and the antioxidant defense protein pathway. Further functional studies with these newly identified proteins can potentially lead to new targets for the therapeutic interventions in patients with DR, diabetic macular edema, or other retinopathies refractory to the current anti-VEGF therapy.

Supplementary Material

Refer to Web version on PubMed Central for supplementary material.

Acknowledgments

The authors thank the Center for Biomedical Informatics of the University of Missouri (Columbia, MO, USA) for assistance in bioinformatics analysis and use of its computer application facilities. Ms. Catherine Brooks J. and Ms. Morey Sharon S. (Mason Eye Institute, University of Missouri, Columbia, Missouri, United States of America) for additional language corrections

Funding

This work was supported by the National Institutes of Health (grant EY027824) and start-up funds from the University of Missouri.

References

1. Maglione D; Guerriero V; Viglietto G; Delli-Bovi P; Persico MG, Isolation of a human placenta cDNA coding for a protein related to the vascular permeability factor. Proc Natl Acad Sci U S A 1991, 88, (20), 9267–71. [PubMed: 1924389]
2. Cunningham F; Van Bergen T; Canning P; Lengyel I; Feyen JHM; Stitt AW, The Placental Growth Factor Pathway and Its Potential Role in Macular Degenerative Disease. Curr Eye Res 2019, 44, (8), 813–822. [PubMed: 31055948]
3. Luttun A; Tjwa M; Moons L; Wu Y; Angelillo-Scherrer A; Liao F; Nagy JA; Hooper A; Priller J; De Klerck B; Compernolle V; Daci E; Bohlen P; Dewerchin M; Herbert JM; Fava R; Matthys P; Carmeliet G; Collen D; Dvorak HF; Hicklin DJ; Carmeliet P, Revascularization of ischemic tissues by PlGF treatment, and inhibition of tumor angiogenesis, arthritis and atherosclerosis by anti-Flt1. Nat Med 2002, 8, (8), 831–40. [PubMed: 12091877]
4. De Ceuninck F; Dassencourt L; Anract P, The inflammatory side of human chondrocytes unveiled by antibody microarrays. Biochem Biophys Res Commun 2004, 323, (3), 960–9. [PubMed: 15381094]
5. Huang H; He J; Johnson D; Wei Y; Liu Y; Wang S; Lutty GA; Duh EJ; Semba RD, Deletion of placental growth factor prevents diabetic retinopathy and is associated with Akt activation and HIF1alpha-VEGF pathway inhibition. diabetes 2015;64:200–212. Diabetes 2015, 64, (3), 1067. [PubMed: 25187372]
6. Verlohren S; Herraiz I; Lapaire O; Schlembach D; Moertl M; Zeisler H; Calda P; Holzgreve W; Galindo A; Engels T; Denk B; Stepan H, The sFlt-1/PlGF ratio in different types of hypertensive pregnancy disorders and its prognostic potential in preeclamptic patients. Am J Obstet Gynecol 2012, 206, (1), 58 e1–8. [PubMed: 22000672]
7. Cianfarani F; Zambruno G; Brogelli L; Sera F; Lacal PM; Pesce M; Capogrossi MC; Failla CM; Napolitano M; Odorisio T, Placenta growth factor in diabetic wound healing: altered expression and therapeutic potential. Am J Pathol 2006, 169, (4), 1167–82. [PubMed: 17003476]
8. Snuderl M; Batista A; Kirkpatrick ND; Ruiz de Almodovar C; Riedemann L; Walsh EC; Anolik R; Huang Y; Martin JD; Kamoun W; Knevels E; Schmidt T; Farrar CT; Vakoc BJ; Mohan N; Chung E; Roberge S; Peterson T; Bais C; Zhelyazkova BH; Yip S; Hasselblatt M; Rossig C; Niemeyer E; Ferrara N; Klagsbrun M; Duda DG; Fukumura D; Xu L; Carmeliet P; Jain RK, Targeting placental growth factor/neuropilin 1 pathway inhibits growth and spread of medulloblastoma. Cell 2013, 152, (5), 1065–76. [PubMed: 23452854]
9. Al Kahtani E; Xu Z; Al Rashaed S; Wu L; Mahale A; Tian J; Abboud EB; Ghazi NG; Kozak I; Gupta V; Arevalo JF; Duh EJ, Vitreous levels of placental growth factor correlate with activity of proliferative diabetic retinopathy and are not influenced by bevacizumab treatment. Eye (Lond) 2017, 31, (4), 529–536. [PubMed: 27886182]
10. Van Bergen T; Etienne I; Cunningham F; Moons L; Schlingemann RO; Feyen JHM; Stitt AW, The role of placental growth factor (PlGF) and its receptor system in retinal vascular diseases. Prog Retin Eye Res 2019, 69, 116–136. [PubMed: 30385175]

11. Latha MS; Saddala MS, Molecular docking based screening of a simulated HIF −1 protein model for potential inhibitors. Bioinformation 2017, 13, (11), 388–393. [PubMed: 29225432]
12. Saddala MS; Lennikov A; Grab DJ; Liu GS; Tang S; Huang H, Proteomics reveals ablation of PlGF increases antioxidant and neuroprotective proteins in the diabetic mouse retina. Sci Rep 2018, 8, (1), 16728. [PubMed: 30425286]
13. Huang H; Lennikov A; Saddala MS; Gozal D; Grab DJ; Khalyfa A; Fan L, Placental growth factor negatively regulates retinal endothelial cell barrier function through suppression of glucose-6-phosphate dehydrogenase and antioxidant defense systems. FASEB J 2019, 33, (12), 13695–13709. [PubMed: 31585507]
14. Breitwieser FP; Muller A; Dayon L; Kocher T; Hainard A; Pichler P; Schmidt-Erfurth U; Superti-Furga G; Sanchez JC; Mechtler K; Bennett KL; Colinge J, General statistical modeling of data from protein relative expression isobaric tags. J Proteome Res 2011, 10, (6), 2758–66. [PubMed: 21526793]
15. Dayon L; Turck N; Kienle S; Schulz-Knappe P; Hochstrasser DF; Scherl A; Sanchez JC, Isobaric tagging-based selection and quantitation of cerebrospinal fluid tryptic peptides with reporter calibration curves. Anal Chem 2010, 82, (3), 848–58. [PubMed: 20058875]
16. Dayon L; Turck N; Scherl A; Hochstrasser DF; Burkhard PR; Sanchez JC, From relative to absolute quantification of tryptic peptides with tandem mass tags: application to cerebrospinal fluid. Chimia (Aarau) 2010, 64, (3), 132–5. [PubMed: 21140904]
17. Elias JE; Gygi SP, Target-decoy search strategy for increased confidence in large-scale protein identifications by mass spectrometry. Nat Methods 2007, 4, (3), 207–14. [PubMed: 17327847]
18. McAlister GC; Nusinow DP; Jedrychowski MP; Wuhr M; Huttlin EL; Erickson BK; Rad R; Haas W; Gygi SP, MultiNotch MS3 enables accurate, sensitive, and multiplexed detection of differential expression across cancer cell line proteomes. Anal Chem 2014, 86, (14), 7150–8. [PubMed: 24927332]
19. Gluck F; Hoogland C; Antinori P; Robin X; Nikitin F; Zufferey A; Pasquarello C; Fetaud V; Dayon L; Muller M; Lisacek F; Geiser L; Hochstrasser D; Sanchez JC; Scherl A, EasyProt--an easy-to-use graphical platform for proteomics data analysis. J Proteomics 2013, 79, 146–60. [PubMed: 23277275]
20. Saddala MS; Lennikov A; Mukwaya A; Fan L; Hu Z; Huang H, Transcriptome-wide analysis of differentially expressed chemokine receptors, SNPs, and SSRs in the age-related macular degeneration. Hum Genomics 2019, 13, (1), 15. [PubMed: 30894217]
21. Thompson A; Schafer J; Kuhn K; Kienle S; Schwarz J; Schmidt G; Neumann T; Johnstone R; Mohammed AK; Hamon C, Tandem mass tags: a novel quantification strategy for comparative analysis of complex protein mixtures by MS/MS. Anal Chem 2003, 75, (8), 1895–904. [PubMed: 12713048]
22. Benjamini Y; Drai D; Elmer G; Kafkafi N; Golani I, Controlling the false discovery ate in behavior genetics research. Behav Brain Res 2001, 125, (1–2), 279–84. [PubMed: 11682119]
23. Thomas PD; Kejariwal A; Campbell MJ; Mi H; Diemer K; Guo N; Ladunga I; Ulitsky-Lazareva B; Muruganujan A; Rabkin S; Vandergriff JA; Doremieux O, PANTHER: a browsable database of gene products organized by biological function, using curated protein family and subfamily classification. Nucleic Acids Res 2003, 31, (1), 334–41. [PubMed: 12520017]
24. Huang HS, M. S; Lennikov A; Mukwaya A; Fan L, Pathway-Focused Gene Interaction Analysis Reveals the Regulation of TGFβ, Pentose Phosphate and Antioxidant Defense System by Placental Growth Factor in Retinal Endothelial Cell Functions: Implication in Diabetic Retinopathy. . Preprints 2019, 2019070140 2019.
25. Huang SH; Hsueh HJ; Jiang YL, Light-addressable electrodeposition of cell-encapsulated alginate hydrogels for a cellular microarray using a digital micromirror device. Biomicrofluidics 2011, 5, (3), 34109–3410910. [PubMed: 22685500]
26. Wamelink MM; Struys EA; Jakobs C, The biochemistry, metabolism and inherited defects of the pentose phosphate pathway: a review. J Inherit Metab Dis 2008, 31, (6), 703–17. [PubMed: 18987987]

27. Fujita H; Aoki H; Ajioka I; Yamazaki M; Abe M; Oh-Nishi A; Sakimura K; Sugihara I, Detailed expression pattern of aldolase C (Aldoc) in the cerebellum, retina and other areas of the CNS studied in Aldoc-Venus knock-in mice. PLoS One 2014, 9, (1), e86679. [PubMed: 24475166]

28. Canete-Soler R; Reddy KS; Tolan DR; Zhai J, Aldolases a and C are ribonucleolytic components of a neuronal complex that regulates the stability of the light-neurofilament mRNA. J Neurosci 2005, 25, (17), 4353–64. [PubMed: 15858061]

29. Buono P; D'Armiento FP; Terzi G; Alfieri A; Salvatore F, Differential distribution of aldolase A and C in the human central nervous system. J Neurocytol 2001, 30, (12), 957–65. [PubMed: 12626877]

30. Dale RC; Candler PM; Church AJ; Wait R; Pocock JM; Giovannoni G, Neuronal surface glycolytic enzymes are autoantigen targets in post-streptococcal autoimmune CNS disease. J Neuroimmunol 2006, 172, (1–2), 187–97. [PubMed: 16356555]

Significance

PlGF (Placental growth factor) is known to play a pivotal role in pathological angiogenesis and inflammation by stimulating endothelial cell migration and by recruiting pericytes and inflammatory cells such as microglia and macrophages. Despite the well-defined pathophysiological roles of PlGF, the underlying molecular and cellular mechanisms are not completely understood, especially the exact relationships between biochemical events and molecular pathways regulated by PlGF, whose inhibition exhibits a protective role in diabetic retinopathy. This study provides new insights into protein expression patterns and enables the identification of many attractive candidates for investigation of PPP pathway role in the activation of the antioxidant defense system in diabetic retinopathy (DR). Our findings suggest that the PPP proteins and antioxidants (PRDX6, HMOX1, NQO1 and YES1) may act as downstream targets of PlGF and may play a decisive role in HREC biological functions in DR.

Highlights

- TMT-labeled quantitative proteomic analysis on human retinal endothelial cells (HRECs), treated anti-PlGF antibody.
- This study identified 305 differentially expressed proteins and potential signaling pathways that are involved in the pentose phosphate pathway (PPP)and antioxidants activity.
- This study indicated that ALDOA, ALDOC, DERA, G6PD, PGLS, RPE, TKT and Prdx are the key factor of the pentose phosphate pathway (PPP) and antioxidants according to the integrated analysis of transcriptomic and proteomic data.
- The result revealed PPP proteins and antioxidants may act as a downstream target of PlGF and may play a decisive role in HREC biological functions in diabetic retinopathy (DR).

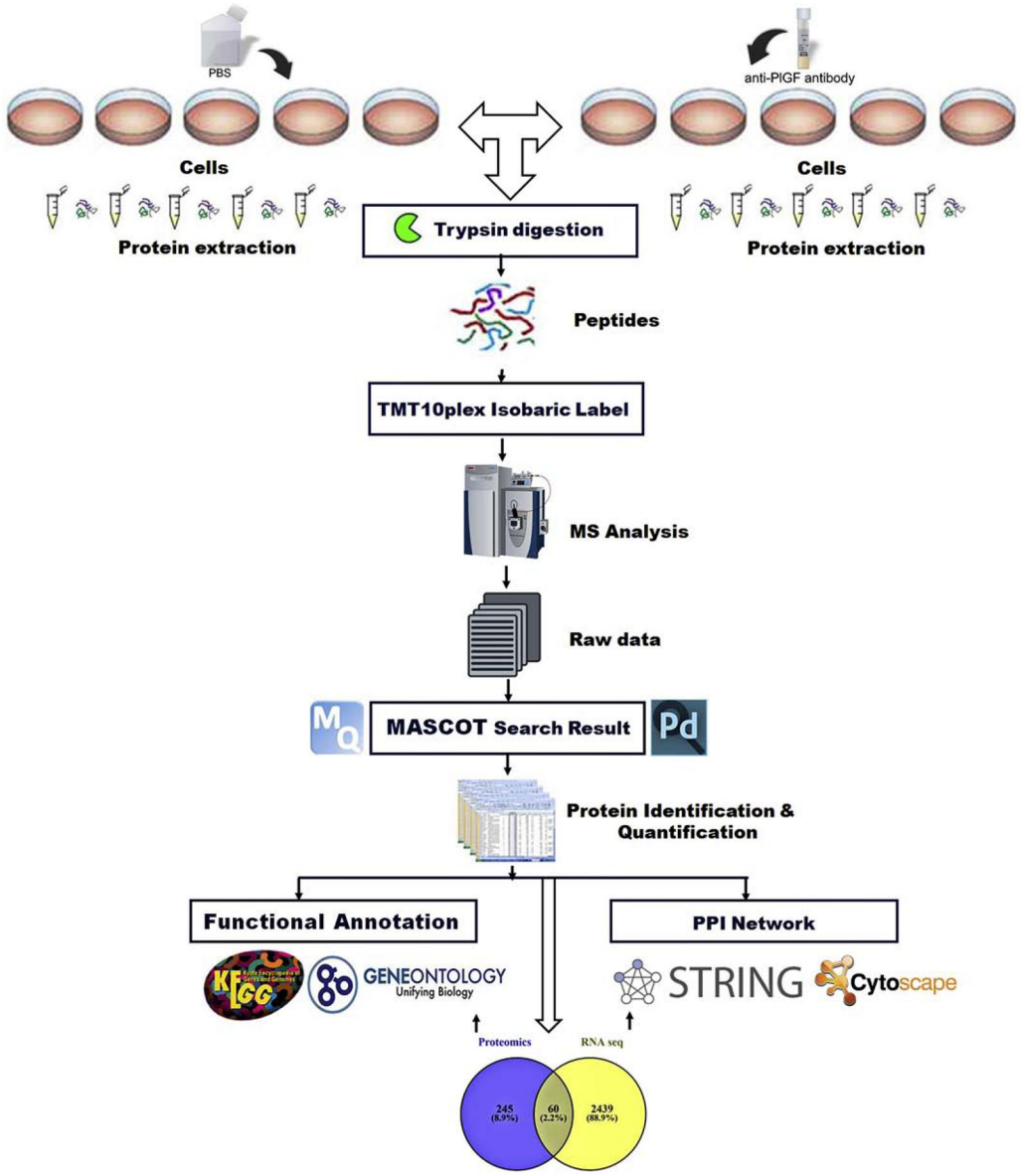

Figure 1:

Schematic of the experimental workflow. HREC cultures were treated with PBS control and anti-PlGF antibody (5 replicates per group). Proteins were extracted, digested with trypsin, and labeled with a specific TMT reagent. The resulting peptide mixtures were labeled with one of the TMT reagents from the 10plex version. The labeled samples were then fractionated by high-pH reverse-phase high-performance liquid chromatography (HPLC) using an Agilent 300 Extend C18 column. Bioinformatics and statistical analyses were performed to identify and quantify the proteins. The differentially expressed proteins (DEPs) were performed gene ontology and functional enrichment analysis. The DEPs were further compared with transcriptome data (RNA-Seq) and annotated.

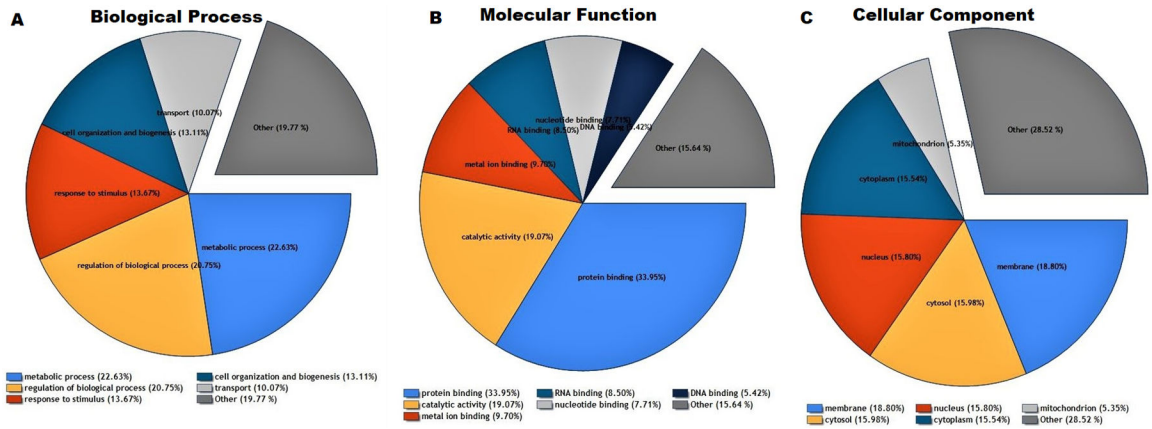

Figure 2:

Gene ontology (GO) analysis illustrates the classification of proteins. Proteins with significant differences between the two groups were subjected to GO classification in terms of biological process (**A**), molecular function (**B**), and cellular compartment (**C**). A GO term was considered significant at p-value < 0.05.

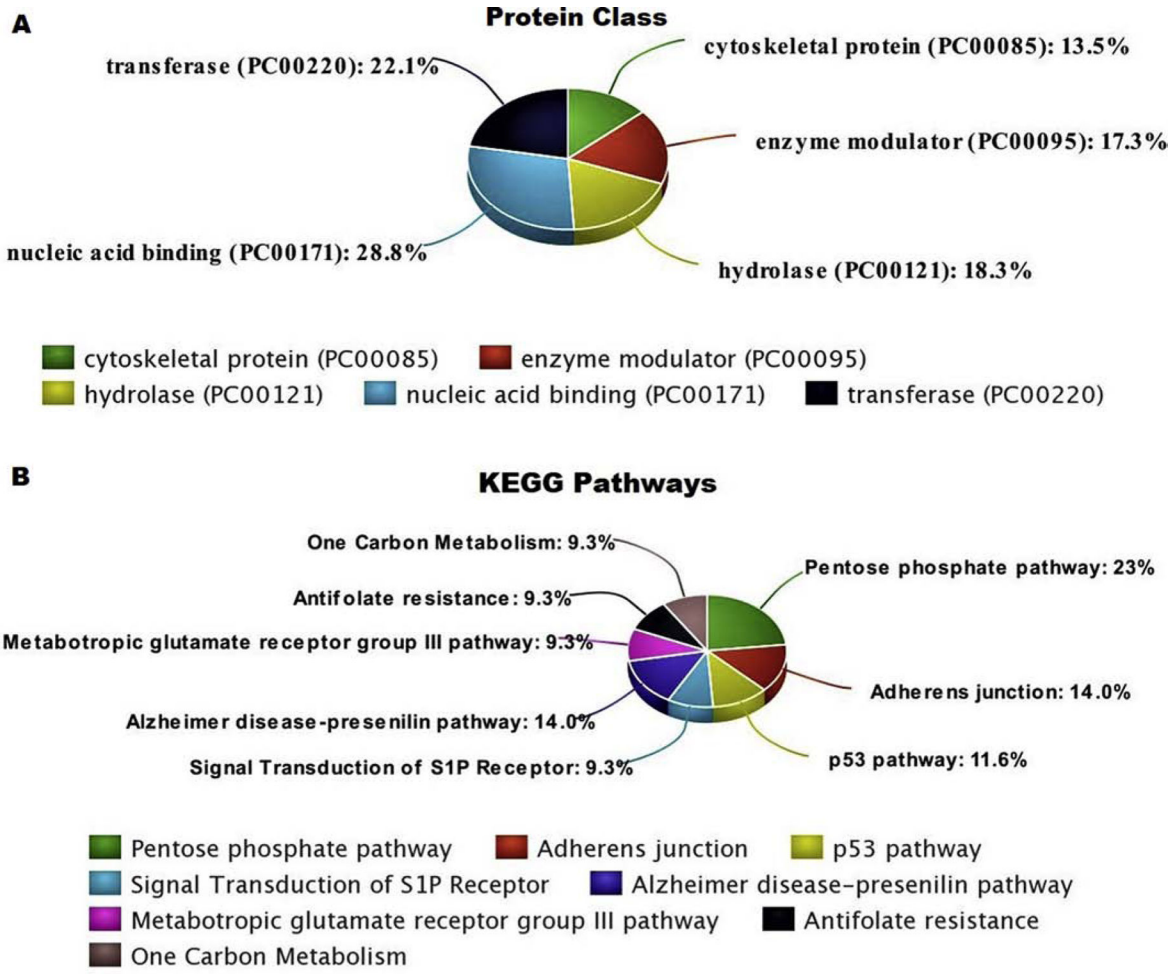

Figure 3:

Proteins with significant differences between the PlGF-ab–treated HREC samples and the HREC control samples were subjected to functional enrichment analysis in terms of protein class (**A**), KEGG pathway analysis (**B**). The results were considered significant at p-value < 0.05.

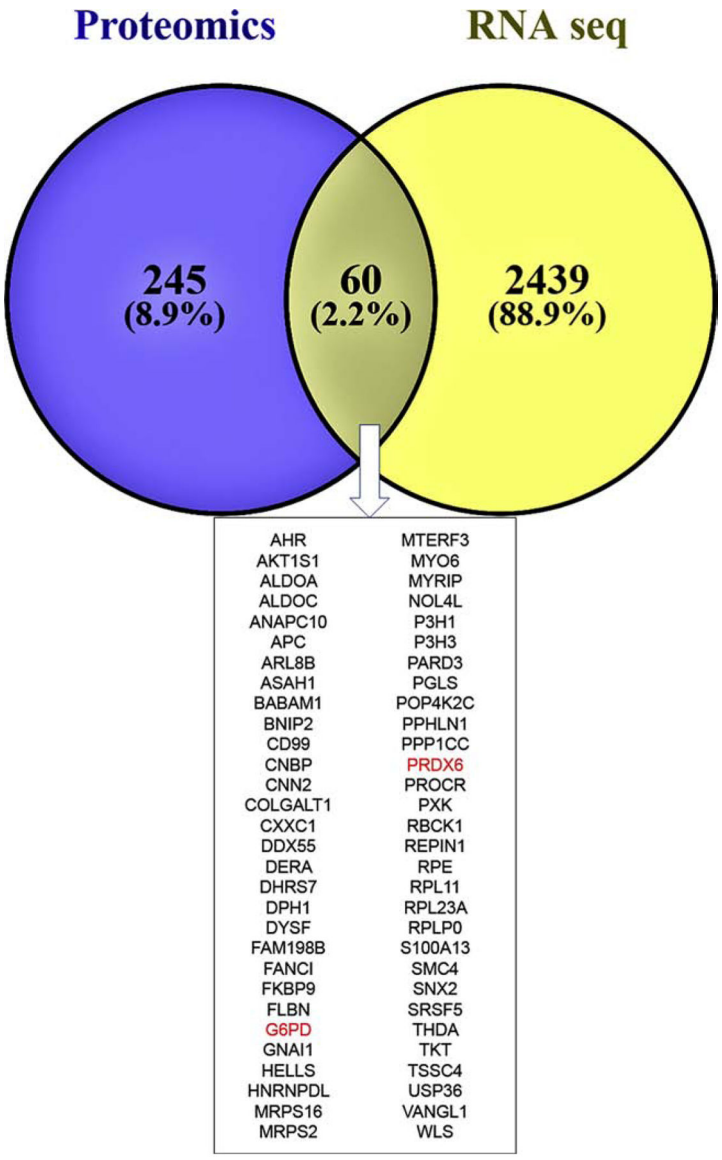

Figure 4:

The Venn diagram illustrates the comparisons of proteomics and transcriptome data of the differentially expressed proteins (DEPs) and differentially expressed genes (DEGs). The Venn diagram showed that 60 proteins overlapped between proteomics and transcriptome data.

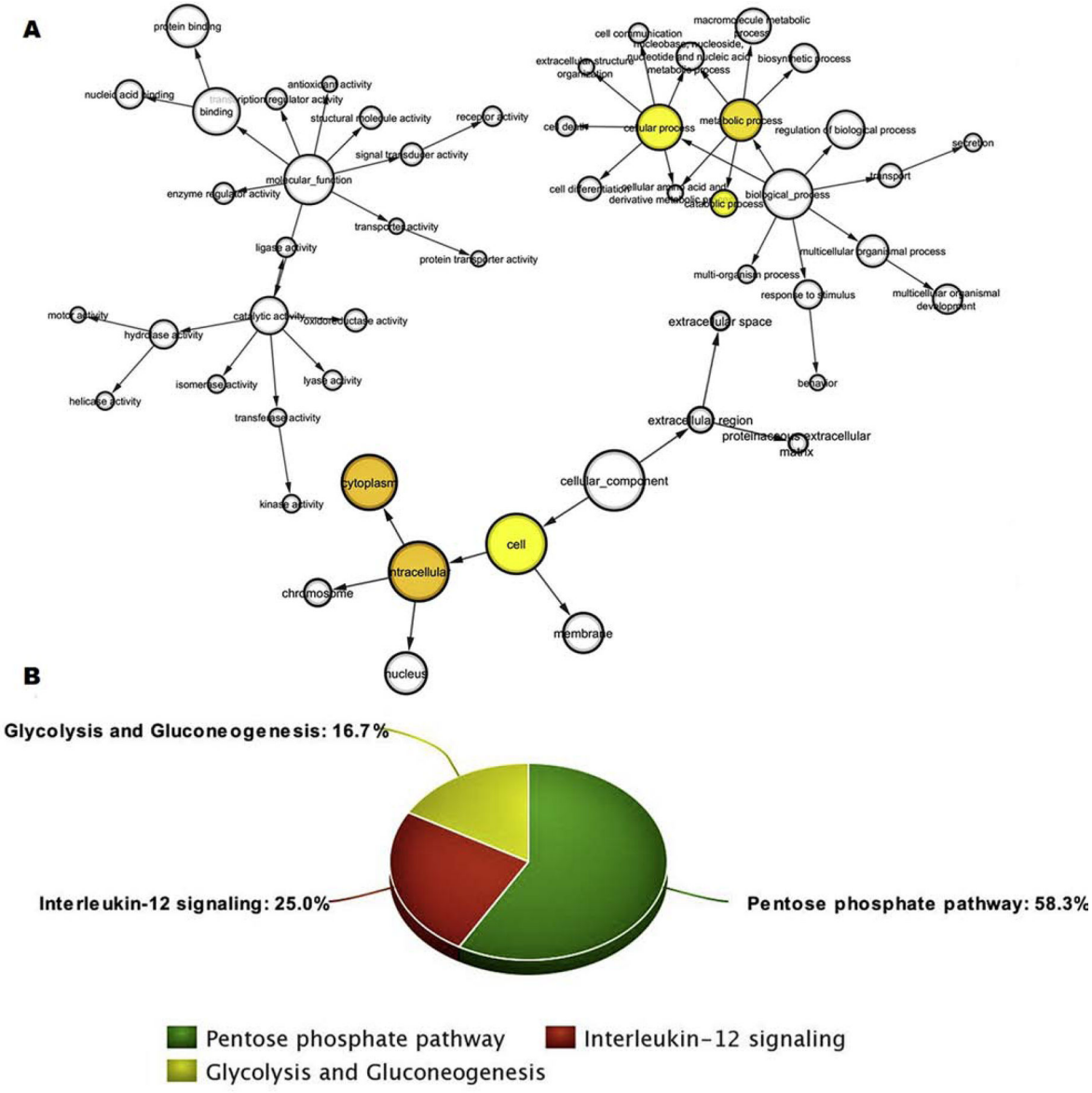

Figure 5:

Gene ontology (GO) analysis illustrates the classification of the 60 overlapped proteins/mRNA transcripts between the proteomics and transcriptome data. (**A**) The common proteins/mRNA transcripts were subjected to GO classification in terms of biological process, molecular function, and cellular compartment. (**B**) KEGG pathway analysis. Note that 58.3 percent of these factors are involved in the pentose phosphate pathway. A GO term was considered significant at p-value < 0.05.

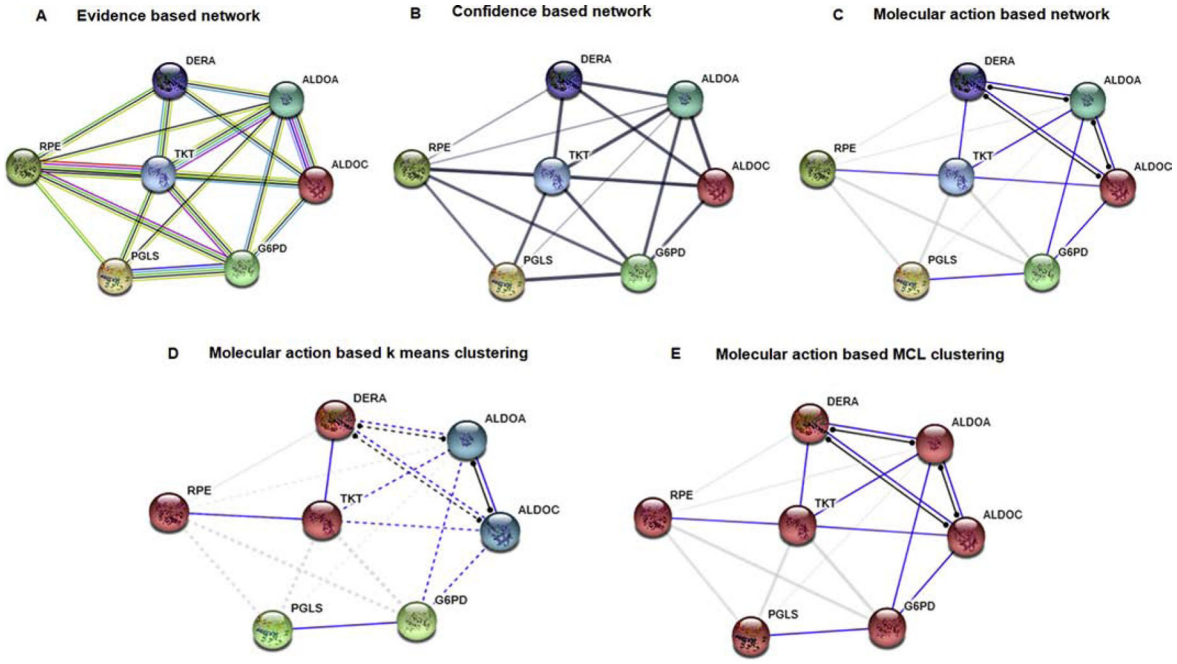

Figure 6:

Protein-protein interaction (PPI) regulatory network of proteins involved in the pentose phosphate pathway (PPP). Differentially expressed proteins of the PPP were combined for building a regulatory network using String software. (**A)** The evidence-based interaction network analysis, (**B**) The confidence-based interaction network analysis, (**C)** The molecular action-based interaction network analysis, (**D**) A k means cluster analysis of the genes. (**E**) A Markov Cluster Algorithm (MCL) cluster analysis of the genes.

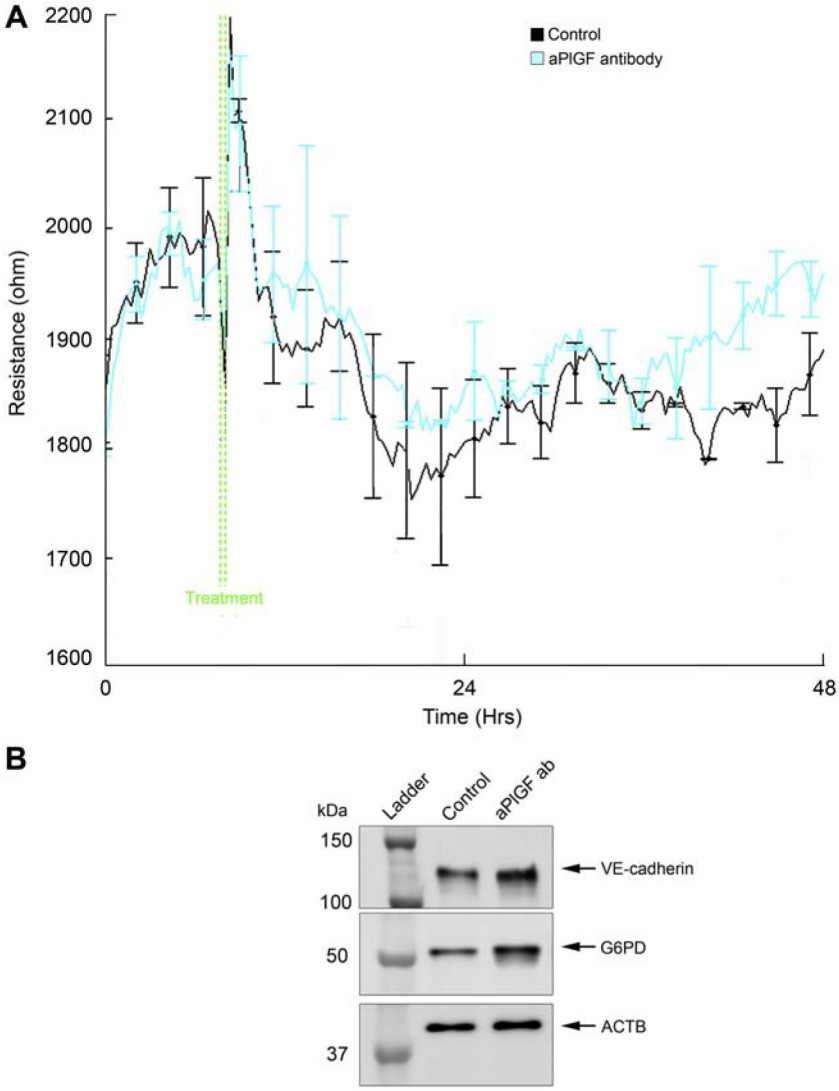

Figure 7:

Transendothelial electrical resistance measurement (TEER) by an electrical cell-impedance sensing system (ECIS) of HREC treated with anti-PLGF antibody and western blot validation of HREC protein extracts. **A**. Treatment with anti-PlGF antibody (PL5D11D4; 25 μg/ml) of HREC cultures resulted in a prominent increase of measured resistance by ECIS, starting 24 h after treatment and becoming prominent by 48 h. **B**. Western blot analysis of VE-cadherin, G6PD in HREC protein extracts treated with (PL5D11D4; 25 μg/ml) collected at 48 hours after the start of the treatment.

Table 1:

List of Pentose phosphate pathway genes, and antioxidant genes along with Ensembl, gene symbol, gene name logFC, p-values in proteomics data analysis.

Ensembl	Gene Symbol	Gene Name	Abundance Ratio (log2)	p-value
ENSG00000149925	ALDOA	aldolase, fructose-bisphosphate A	−0.3098081	0.05
ENSG00000109107	ALDOC	aldolase, fructose-bisphosphate C	−0.3773762	0.03
ENSG00000023697	DERA	deoxyribose-phosphate aldolase	0.9723172	0.01
ENSG00000160211	G6PD	glucose-6-phosphate dehydrogenase	0.2379935	0.01
ENSG00000130313	PGLS	6-phosphogluconolactonase	−0.8096812	0.01
ENSG00000197713	RPE	ribulose-5-phosphate-3-epimerase	0.5650684	0.02
ENSG00000163931	TKT	Transketolase	0.2392153	0.01
Antioxidant genes				
ENST00000470017	PRDX6	peroxiredoxin 6	0.7948333	0.04
ENSG00000100292	HMOX1	heme Oxygenase 1	0.1752908	0.02
ENSG00000181019	NQO1	NAD(P)H Quinone Dehydrogenase 1	0.1932262	0.05
ENSG00000176105	YES1	YES Proto-Oncogene 1, Src Family Tyrosine Kinase	0.8682562	0.04